



Direct radiative effects of black carbon and brown carbon from Southeast Asia biomass burning with the WRF-CMAQ two-way coupled model[☆]

Yeqi Huang^a, Xingcheng Lu^c, Zhenning Li^a, Jimmy C.H. Fung^{a,b,*}, Yuhang Wang^d,
Yiang Chen^a

^a Division of Environment and Sustainability, The Hong Kong University of Science and Technology, Clear Water Bay, Kowloon, Hong Kong SAR, China

^b Department of Mathematics, The Hong Kong University of Science and Technology, Clear Water Bay, Kowloon, Hong Kong SAR, China

^c Department of Geography and Resource Management, The Chinese University of Hong Kong, Sha Tin, Hong Kong SAR, China

^d School of Earth and Atmospheric Sciences, Georgia Institute of Technology, Atlanta, GA, USA

ARTICLE INFO

Keywords:

Black and brown carbon
Direct aerosol radiative effect
The Weather Research Forecast-Community
Multiscale Air Quality Modeling System (WRF-
CMAQ) two-way coupled model
Biomass burning emission
Southeast Asia

ABSTRACT

Black carbon (BC) and brown carbon (BrC) are significant light-absorbing components of particulate matter that impact weather and climate. Biomass burning (BB) and biofuel (BF) emissions in Southeast Asia are key global sources of BC and BrC. This study utilizes the Weather Research and Forecasting-Community Multiscale Air Quality (WRF-CMAQ) model, integrating a BrC module for the first time, alongside the Global Fire Emissions Database Version 4, to assess the direct radiative effect (DRE) of BC and BrC in March 2015 over Southeast Asia. The novel BrC module parameterizes light absorption based on the BB BC to organic aerosol (OA) ratio in each model grid and time step, aligning better with smog chamber experiments than default coefficients. Results show that BC DRE affects clear sky net radiation at the top of the atmosphere, reaching 14.6 W/m² in Indochina and 5.1 W/m² in southern China, while BrC DRE reaches 1.9 W/m². Additionally, BC and BrC DRE induce a cooling effect at the Earth's surface, with the maximum reduction of the clear sky downward shortwave radiation by -36.9 W/m² and -5.2 W/m², respectively. BC and BrC lead to a tiny decrease (<0.1 °C) in surface temperature and an increase in upper air temperature. Surface O₃ concentration tends to slightly decrease (<1.0 ppbv) due to the DRE of BC and BrC. In comparison to studies using the default coefficient, this result contributes to a more nuanced understanding of the interactions between BC, BrC, and radiation.

1. Introduction

Aerosols, including sulfate, nitrate, ammonium, black carbon (BC), and organic aerosol (OA), are significant environmental pollutants that can have adverse effects on visibility and human health (Johnston et al., 2012; Chen et al., 2017; Reddington et al., 2021). These aerosols can influence the Earth's energy balance through both direct and indirect radiative effects. Generally, non-light-absorbing aerosols such as sulfate and nitrate tend to reflect solar radiation back into space, while dark-colored aerosols like BC have the capability to absorb substantial amounts of light (Charlson et al., 1992; Moosmüller et al., 2009; Bahadur et al., 2012; Qin et al., 2018). OA was initially characterized as 'white' in the atmosphere, which can only scatter the sunlight and cool the climate. However, a great number of OA has been reported to

effectively absorb light in the ultraviolet-visible range (Pöschl, 2005; Zhang et al., 2017; Yan et al., 2018), and this fraction of OA was firstly named as brown carbon (BrC) by Andreae and Gelencsér (2006). The absorptivity of BC and BrC can heat the atmosphere, reduce the reflectivity of snow and ice by depositing on them, and alter the microphysical properties of clouds (Guyon et al., 2005; US Environmental Protection Agency, 2012; Bond et al., 2013). Furthermore, the alteration in light and meteorological conditions can influence the atmospheric oxidizing capacity, and the formation and degradation of pollutants. These changes will affect the production rate of ozone (O₃) and secondary organic aerosols (Cheng et al., 2014; Jo et al., 2016; Li et al., 2018), as well as lead to the persistent presence of polyurethane plastics in environmental systems (Tian et al., 2024a; Cui et al., 2024; Tian et al., 2024b).

[☆] This paper has been recommended for acceptance by Krishna Vadrevu

* Corresponding author. Division of Environment and Sustainability, The Hong Kong University of Science and Technology, Clear Water Bay, Kowloon, Hong Kong SAR, China.

E-mail address: majfung@ust.hk (J.C.H. Fung).

<https://doi.org/10.1016/j.envpol.2024.125425>

Received 12 May 2024; Received in revised form 2 October 2024; Accepted 28 November 2024

Available online 29 November 2024

0269-7491/© 2024 Elsevier Ltd. All rights reserved, including those for text and data mining, AI training, and similar technologies.

Currently, our understanding of BC is relatively comprehensive, and the radiative effect of BC has been widely incorporated into climate and regional models (Bond and Bergstrom, 2006; Ramanathan and Carmichael, 2008; Wu et al., 2008; Bond et al., 2011). As a significant contributor to global warming, UNEP/WMO assessment (UNEP and WMO, 2011) evaluated a number of studies on the climate impact of BC and reported the global annual average direct radiative effect (DRE) of BC ranged from +0.2 to +0.9 W/m². Through extensive field observations and laboratory simulations of carbonaceous aerosols, the understanding of BrC has significantly advanced over the years (Mukai and Ambe, 1986; Pöschl, 2005; Andreae and Gelencsér, 2006), and solar absorption of BrC was found to be comparable to that of BC near ultra-violet wavelengths in some cases (Bahadur et al., 2012; Chung et al., 2012; Kirchstetter and Thatcher, 2012; Saleh et al., 2018). However, different from BC, which consists of pure carbon in several linked forms with uniform physicochemical and optical properties, BrC is a more complex mixture of organic compounds. BrC can originate from incomplete combustion of biomass and biofuels (BF) (Hecobian et al., 2010; Saleh et al., 2013; Xie et al., 2018), as well as chemical reactions of volatile and semi-volatile organic compounds (e.g., aromatic hydroxyl acid) in the atmosphere (Wu et al., 2016). These compounds possess diverse structures and properties, which can influence their optical characteristics. The complexity of BrC poses challenges in studying and comprehending its properties and impact on the environment and human health. Despite integrating BrC into models poses challenges due to its complex nature, the significance of BrC observed in the field and in laboratory experiments has still prompted an increasing number of studies to attempt to incorporate the radiative effects of BrC into models (Park et al., 2010; Saleh et al., 2015; Brown et al., 2018). The discussion on the optical properties of BrC is the most effective from a practical standpoint, which has also been highly considered in the models. Some studies have assumed that a portion of the OA is BrC and have assigned a new optical property for BrC to differentiate BrC from non-absorbing OA (Feng et al., 2013; Zhang et al., 2020). However, the proportion of BrC in OA, which is impacted by fuel types, burning conditions, etc., can vary greatly, and a fixed BrC optical property does not adequately represent the complexity of BrC. Benefit from field observations and laboratory simulations, the BrC absorptivity and the wavelength dependence of the absorptivity from biomass burning (BB) and BF can be parameterized as a function of the BC to OA ratio, regardless of burning types and conditions (Saleh et al., 2014; Wang et al., 2016). This parameterization has been widely used in modelling studies. With the BrC parameterization scheme, most studies simulated BrC on a global scale and the simulated BrC DRE ranged from +0.03 to +0.6 W/m² (Saleh et al., 2015; Brown et al., 2018; Wang et al., 2018; June et al., 2020).

Most model-based studies on BrC DRE have primarily focused on climatic or global impacts, with few investigating local or short-term scales. However, similar to BC, BrC is prevalent in particular geographic regions, such as Southeast Asia, South America, Africa, where high levels of biomass burning occur, leading to a substantial contribution of both BC and BrC DRE in these areas. Previous studies found that from a regional scale perspective, the BC DRE can be more than 8 W/m² (Hansen et al., 2005; Zhang et al., 2009; Lin et al., 2014; Li et al., 2022), which is much significant than that from a global scale. Few studies have found that BrC DRE can reach 1 W/m² in a regional scale (Park et al., 2010; Zhang et al., 2020). Southeast Asia is a diverse region characterized by its tropical climate, rich biodiversity, and varied geographical features. Biomass burning from land clearing for agriculture and forest management, is prevalent in countries like Indonesia and Malaysia (van Marle et al., 2017). This practice significantly contributes to the emission of BC and BrC, both of which are light-absorbing aerosols that impact air quality and climate during the springtime due to frequent BB activities in Indochina. Our previous study (Huang et al., 2023) investigated the emission and direct aerosol radiative effects of BB in Southeast Asia, and revealed that BB activities in March significantly

impacted local meteorological conditions and air quality, as well as downwind regions such as Southern China. However, the previous study did not account for the DRE of BrC.

In this study, for the first time, we integrated a parameterization of BrC DRE into the Weather Research Forecast-Community Multiscale Air Quality Modeling System (WRF-CMAQ) two-way coupled model to improve our comprehension of the influence of BrC's solar radiation absorption on meteorology and air quality. In comparison to studies using the default coefficient, this result contributes to a more nuanced understanding of the interactions between BC, BrC, and radiation. The WRF and CMAQ models are widely used in meteorological and air quality studies, respectively (Dong and Fu, 2015; Huang et al., 2018; Takami et al., 2020; Huang et al., 2021), and they have been continuously updated to benefit the related research and applications. We anticipate that this study will serve as a reference for model developers and researchers investigating the impact of BC and BrC DRE at regional and short-term scales.

2. Data and method

2.1. Model introduction and configuration

A introduction of WRF and CMAQ models is included in the [Supplementary Text S1](#). However, these models have traditionally operated independently (depicted in black in [Fig. 1](#)), lacking information exchange between them as the WRF provides meteorological fields to CMAQ in a unidirectional manner. The WRF-CMAQ two-way coupled model [Wong et al. \(2012\)](#) is an advanced modeling system which utilizes a “feedback” coupler (depicted in blue in [Fig. 1](#)) to establish a feedback path between meteorological processes and chemical reactions. This coupling mechanism is designed to maintain the independence and functionality of both the WRF model and the CMAQ model. In the coupled system, WRF and CMAQ are simultaneously integrated and information from CMAQ (like aerosol concentration) is passed into the “feedback” module so that the chemistry can impact the weather. In the feedback module, a subroutine incorporating the Rapid Radiative Transfer Model for Global Circulation Model (RRTMG) calculates the aerosol optical properties, including extinction optical depth, single scattering albedo, asymmetry parameter, and forward scattering fraction, in 14 shortwave spectral bands. The aerosols in WRF-CMAQ are divided into five groups: water-soluble aerosols, sea salt, water-insoluble aerosols, elemental carbon (i.e. BC), and water. Each group has its own refractive and extinction coefficients, which are obtained from the Optical Properties of Aerosols and Clouds ([Hess et al., 1998](#)) database using linear interpolation to match the central wavelength of the RRTMG wavelength intervals. The extinction and scattering coefficients, as well as the asymmetry factor, are calculated using the efficient Gauss-Hermite numerical-quadrature method. This method integrates the Bohren & Huffman Mie codes over log-normal size distributions representing the Aitken, accumulation, and coarse modes. All BC is coated with a well-mixed shell composed of other aerosols, which is called core-shell (BC-other aerosols) morphology.

In this study, we utilized the WRF version 4.3 and CMAQ version 5.3.3 models to develop the WRF-CMAQ coupled model, which incorporates the direct aerosol radiative forcing to investigate the radiation effects of BC and BrC over Southeast Asia. The study area is a 12-km horizontal resolution domain covering southern China and Indochina ([Fig. 2](#)), and the hybrid sigma-pressure difference vertical coordinate system is employed with 38 vertical layers. The WRF model and radiation module timesteps are set to 30 seconds, and the WRF and CMAQ models are coupled every 10 minutes. The detailed model configurations are summarized in [Table 1](#), which is consistent with our previous study ([Huang et al., 2023](#)). To account for the significant radiative effect of BC, it is considered independently in the model. However, for BrC, it is incorporated into the water-insoluble aerosol category, although the average extinction coefficients might not sufficiently capture BrC's

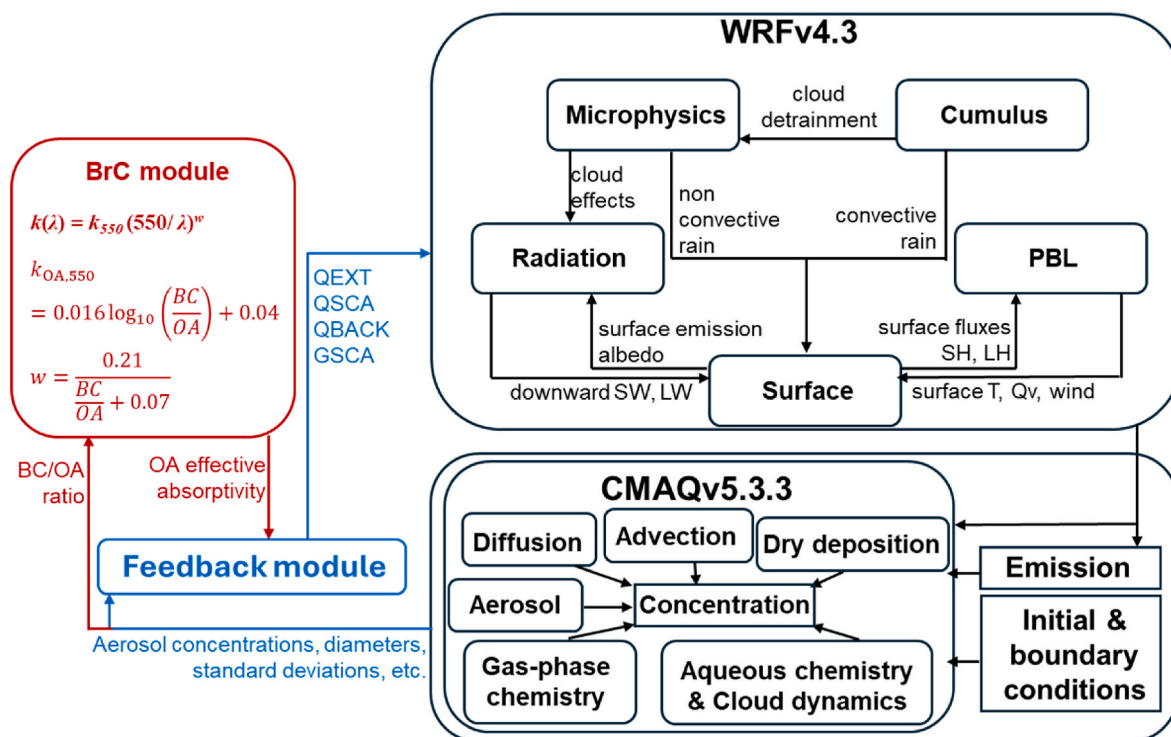


Fig. 1. A schematic diagram of WRF and CMAQ models (depicted in black), the WRF-CMAQ coupled model coupled by feedback module (depicted in black and blue), and the updated BrC module in this study (depicted in red). (For interpretation of the references to color in this figure legend, the reader is referred to the Web version of this article.)

optical properties. In Section 2.3, we will provide an overview of how the BrC module was integrated into the model workflow. Based on our previous study, the impact of BB from the Indochina region was not prominent in April. Therefore, we focused on the month of March 2015 as the study period.

We designed and conducted three sets of experiments:

1. CTRL: includes both BC and BrC direct radiation effects.
2. BrC_OFF: Considers only BC direct radiation effect, with BrC radiation effect turned off.
3. BC_OFF: Considers only BrC direct radiation effect, with BC radiation effect turned off.

2.2. Emission inventories

Anthropogenic emissions data is obtained from the Emissions Database for Global Atmospheric Research (EDGAR, <https://data.jrc.ec.europa.eu/dataset/377801af-b094-4943-8fdc-f79a7c0c2d19>; Crippa et al., 2019; Crippa et al., 2020) version 5 for the base year 2015, with a grid resolution of 0.1° × 0.1°. The BB emission for 2015 is extracted from the Global Fire Emissions Database (GFED, https://daac.ornl.gov/VEGETATION/guides/fire_emissions_v4.html; Randerson et al., 2017) version 4. The injection height of BB smoke plumes, which significantly influences the long-range transport of BC and BrC, is parameterized using the Western Regional Air Partnership (WRAP) method (Air Sciences, 2005). Biogenic emission is simulated by the Model of Emissions of Gases and Aerosols from Nature (MEGAN; Guenther et al., 2020) version 3.1. For more detailed information on the data processing of EDGAR, GFED, BB plume injection height, and biogenic emissions, as well as model evaluation, please refer to Huang et al. (2023) and Text S2.

In this study, the BF emission is also considered because it contributes considerably to BC and BrC. The BF emission data is obtained from the Regional Emission Inventory in Asia (REAS, <https://www.nies.go.jp/REAS/index.html>; Kurokawa and Ohara, 2020) version 3.2 for the base year 2015. The database provides the annual total BF emissions for each province/state in Asian countries. Nine emission species from the database are allocated to the Carbon Bond 6 (CB6) gas-phase mechanism and the Aero7 (AE7) aerosol mechanism for CMAQ-ready input. The annual total emission amount is distributed equally across each day and divided into hourly emission rates based on human activity frequency. Additionally, the data are interpolated to a spatial resolution of 12 km and adjusted to an appropriate vertical structure consistent with the model system.

Fig. S1 shows the average BB and BF emission ratios in March 2015. BB dominates the BC and OA emissions over the Indochina Peninsula, while BF emissions are mainly distributed over Bangladesh and mainland China. BB emissions exhibit a more concentrated emission intensity compared to BF emissions, implying higher local BrC concentrations from BB sources. Furthermore, BB emissions can be transported into the upper atmosphere and impact downstream areas (Huang et al., 2023), while BF emissions may primarily affect local regions because it has been allocated in the surface layer in this study. However, the BC to OA ratio (Fig. 3 (a), introduced in Section 2.3) of BF suggests a stronger extinction coefficient for BF emissions than for BB emissions.

Fig. S1 shows the average BB and BF emission ratios in March 2015. BB dominates the BC and OA emissions over the Indochina Peninsula, while BF emissions are mainly distributed over Bangladesh and mainland China. BB emissions exhibit a more concentrated emission intensity compared to BF emissions, implying higher local BrC concentrations from BB sources. Furthermore, BB emissions can be transported into the upper atmosphere and impact downstream areas (Huang et al., 2023), while BF emissions may primarily affect local regions because it has been allocated in the surface layer in this study. However, the BC to OA ratio (Fig. 3 (a), introduced in Section 2.3) of BF suggests a stronger extinction coefficient for BF emissions than for BB emissions.

2.3. BrC module

In the present study, the default scheme in the WRF-CMAQ, which assigns OA as the water-insoluble aerosol with an averaged extinction coefficient, has been substituted by a scaling module, according to the study of Saleh et al. (2014). To be specific, the optical property can be described by the complex refractive index ($m = n + ik$), where n represents the scattering efficiency, and k represents the extinction efficiency. The wavelength dependence of k can be approximately expressed as an exponent of the power law ($k(\lambda) = k_{550} (550/\lambda)^w$), where k_{550} is k at 550 nm, λ represents the specific wavelength, and w describes the wavelength dependence of k . Saleh et al. (2014) reported that the

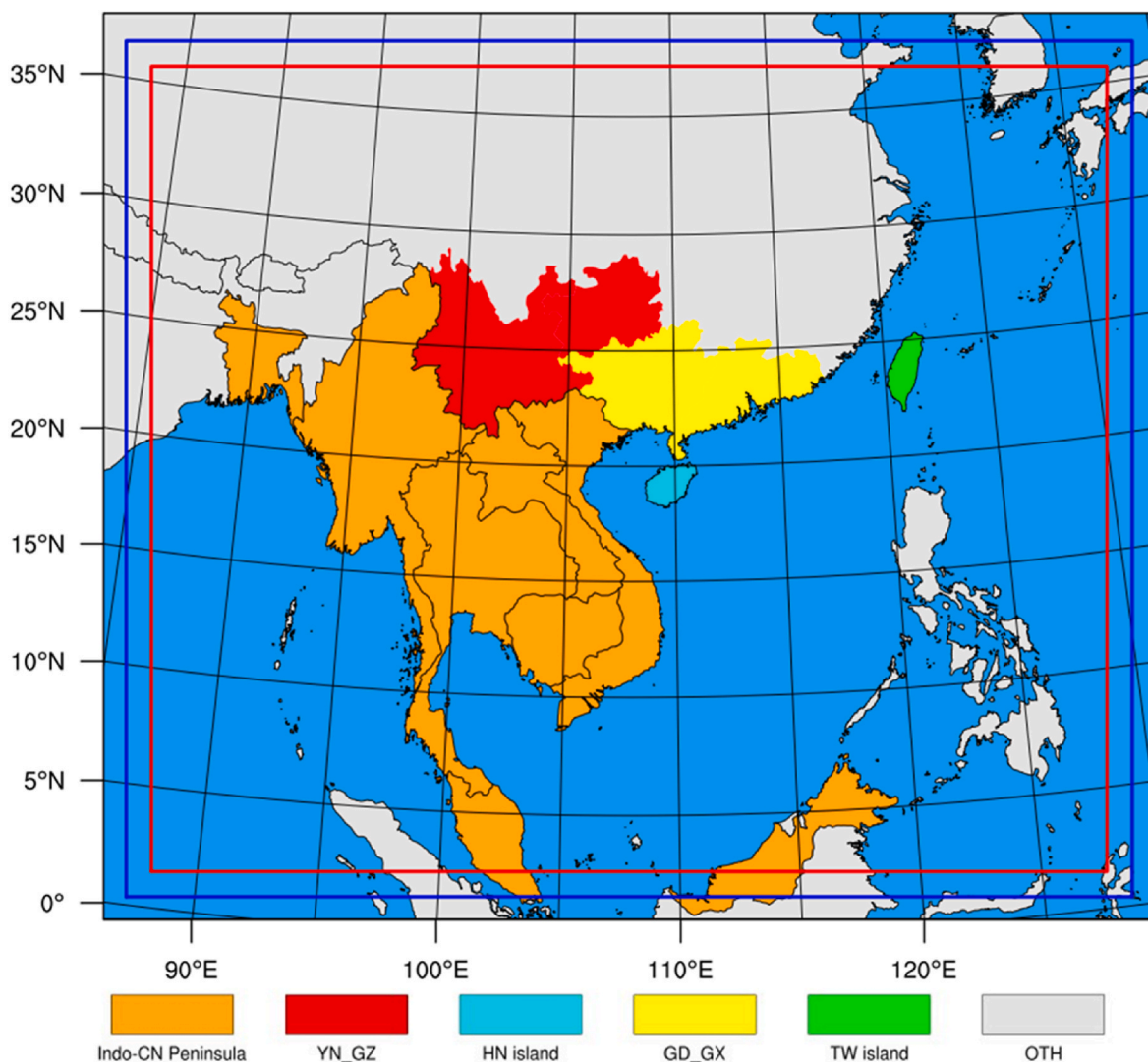


Fig. 2. WRF (red box) and CMAQ (blue box) simulation domains. The six study regions are marked by different colors, as follows: the Indochinese Peninsula (Indo-CN, orange), the Yunnan–Guizhou Plateau (YN_GZ, red), Hainan Island (HN, turquoise), Southern China (GD_GX, yellow), Taiwan Island (TW, green), and other regions (OTH, gray). (For interpretation of the references to color in this figure legend, the reader is referred to the Web version of this article.)

effective absorptivity at 550 nm of OA ($k_{OA,550}$) and the wavelength dependence of k_{OA} could be parameterized by the ratio of BC to OA (BC/OA), as expressed respectively by Equations (1) and (2) below:

$$k_{OA,550} = 0.016 \log_{10} \left(\frac{BC}{OA} \right) + 0.04 \quad (1)$$

$$w = \frac{0.21}{\frac{BC}{OA} + 0.07} \quad (2)$$

The function of w is to extend the k_{OA} from 550 nm to the full spectrum. In Equations (1) and (2), the OA effective absorptivity is parameterized as a function of BC/OA ratio of the BB and BF emissions. The updated BrC module (depicted in red in Fig. 1) retrieves the BC and OA concentrations of BB and BF from a pre-prepared file. The parameterization code then adjusts the imaginary part of the refractive index at the real-time wavelength based on the calculated BC/OA ratio at each time step and grid point. Saleh et al. (2014) reported that the BC/OA ratios in equations (1) and (2) range from 0.01 to 0.5. To independently determine the BB and BF concentrations, two simulations are conducted: one with BB and BF emissions and one without. The difference in BC and OA concentrations between these simulations is attributed to BB and BF emissions. Implementing this function in the WRF-CMAQ model offers

several advantages. Firstly, it eliminates the need for a BrC emission inventory, which is often unavailable. Additionally, it does not require numbers of specific BrC aerosol optical properties or the consideration of BrC formation through other chemical processes. Moreover, the changes to the model structure are minimal, reducing potential errors.

Fig. 3 (a) displays the monthly average BC/OA ratio across the research domain. It can be observed that in most Indochina regions, which are hotspots of BB emissions, the ratio is around 0.15, except in Myanmar, where it can exceed 0.2. In regions dominated by BF emissions, such as China, the ratio is around 0.17. Please note that the ratio shown in this figure represents an average value, while the actual input into the model varies hourly as described earlier. Fig. 3 (b) illustrates the OA extinction coefficients as a function of wavelength (with the x-axis reversed). The blue curve represents the default water-insoluble aerosol extinction coefficients in the WRF-CMAQ model, while the other curves depict the OA effective extinction coefficients. The parameterized OA effective absorptivity varies with the BC/OA ratio. It is observed that as the wavelength decreases, the OA extinction coefficients increase. When compared to the default WRF-CMAQ scheme, an increase in the BC/OA ratio causes a significant rise in the $k_{OA,550}$ value indicating a “darker” BrC when higher BC component dominates. The relationship between BrC absorption and the BC/OA ratio has been confirmed through

Table 1
Model configuration.

Domain Setting	
horizontal resolution	12 × 12 km
vertical resolution	38 sigma-pressure hybrid levels with a top pressure of 50 mb
WRF configuration	
version	v4.3
cloud microphysics	Efficient WRF single-moment 3-class
longwave & shortwave radiation	RRTMG
land-surface process	Pleim–Xiu land-surface model
planetary boundary layer scheme	ACM2
cumulus	Grell 3D
parameterization	
grid nudging	On
model timesteps	30 s
radiation timesteps	10 min
WRF driven data	6-hourly National Centers for Environmental Prediction Final operational global analysis data (http://rda.ucar.edu/datasets/ds083.2/) on 1° × 1° grids
CMAQ configuration	
version	v5.3.3
gas-phase chemistry mechanism	CB6r3 with Euler backward iterative solver
aerosol mechanism	AE7
dry deposition	m3dry
advection	WRF_CONS
vertical diffusion	ACM2_m3dry
coupled frequency	20
initial and boundary conditions	seasonal average Hemispheric CMAQ Output in 2016 over the northern hemisphere (https://drive.google.com/file/d/15Vt6f5WuyN8RiLRjTKeQUHjYbZ6QCrA/view)
emission data	EDGAR version 5 for the base year 2015, with a grid resolution of 0.1° × 0.1° (https://data.jrc.ec.europa.eu/dataset/377801af-b094-4943-8fdc-f79a7c0c2d19). The Global Fire Emissions Database (GFED, https://daac.ornl.gov/VEGETATION/guides/fire_emission_s_v4.html ; Randerson et al., 2017) version 4 for the BB emission in 2015 Regional Emission Inventory in Asia (REAS, https://www.nies.go.jp/REAS/index.html) version 3.2 for BF emission in 2015 MEGANv3.1 for biogenic emission

laboratory studies of biomass and biofuel combustion, field observations, and comparisons of climate-model outputs with satellite observations (Saleh et al., 2014; Saleh et al., 2015; Saleh, 2020). The real part of the refractive index remains consistent with the default water-insoluble aerosols in the model system, ranging from 1.168 to 1.53 at different wavelengths.

3. BC and BrC absorption directive radiative effect

Based on the model experiments, we provide the following interpretation of the radiative absorption effects of BC and BrC: The CTRL simulation represents the combined synergistic effect of BC and BrC. By comparing it with the BC_OFF simulation, we can isolate and quantify the light absorption effect of BC (BC DRE). Similarly, the difference between CTRL and BrC_OFF simulations represents the light absorption effect of BrC (BrC DRE). To better understand the regional impacts of BC and BrC, we divide the model domain into six study regions, each represented by a different color in Fig. 2. These regions are as follows: the Indochina Peninsula (Indo-CN), Yunnan and Guizhou (YN_GZ), Hainan Island (HN), Guangdong and Guangxi (GD_GX), Taiwan Island (TW), and other regions (OTH). In this study, the impact of BC and BrC DRE is closely linked to solar radiation. To facilitate observation of these effects, we focus on a specific local time period from 10 a.m. to 5 p.m. for our calculations. The model performance evaluation of the CTRL simulation can refer to Text S3.

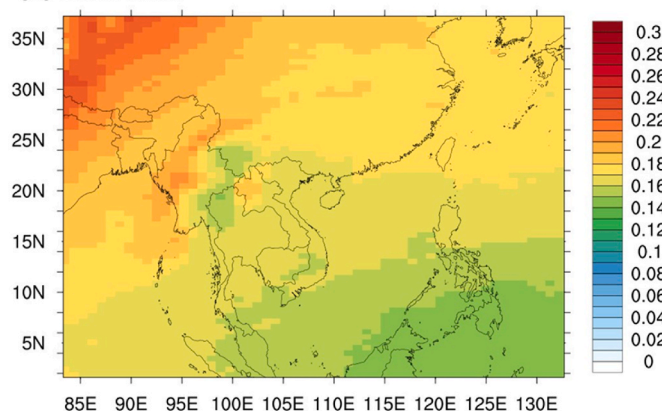
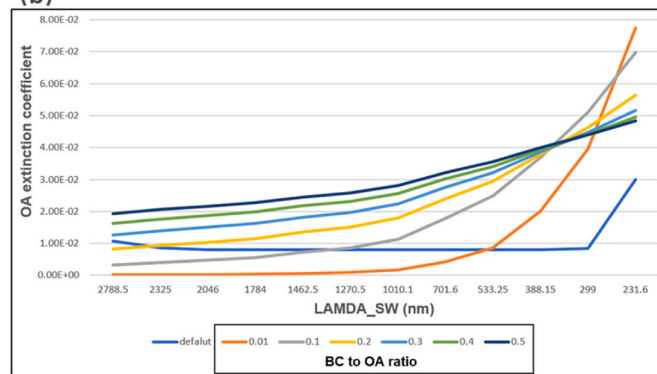
(a) BC/OA ratio**(b)**

Fig. 3. Default insoluble aerosol extinction coefficient and parameterized OA effective absorptivity.

3.1. Impact of BC and BrC DRE on radiation

3.1.1. Monthly average

Fig. 4 (a–c) show the monthly mean clear sky net radiation (shortwave + longwave) flux at the top of the atmosphere (TOA) in March 2015, while Fig. 4 (d–f) show the monthly mean clear sky downward direct shortwave flux on the surface. It is important to note that the figures use a plate carrée map projection for faster visualization and reduced distortion in tropical regions. Consequently, the WRF domain is embedded within the plot domain due to its Lambert projection. The analysis focuses on clear sky radiation flux to eliminate the influence of clouds. In Fig. 4 (a–d), the CTRL simulation effectively captures the spatial distribution pattern of clear sky TOA net radiation flux and downward shortwave flux. Fig. 4 (a) shows high values over the lower latitudes, indicating efficient absorption by tropical oceans. Scattered low values over the Tibetan Plateau indicate the presence of snow cover at high altitudes, which reflects shortwave radiation back to space. Fig. 4 (d) reveals a distinct distribution of solar radiation intensity, with the downward shortwave flux gradually decreasing from south to north in March. The Yunnan and Tibetan Mountain regions exhibit high values due to their elevated altitudes.

Fig. 4 (b, c) demonstrate that both BC and BrC exert significant radiative forcing in the atmospheric system. Generally, BC and BrC absorption DRE contribute positively to the clear sky net radiation at the TOA, indicating a warming effect on the Earth system. Specifically, the maximum, minimum, and average values in the six study regions can be found in Table S2. Fig. 4 (b) illustrates that the BC and BrC DRE impacts can reach as high as 14.6 and 1.9 W/m², respectively, with regional averages of 2.7 and 0.6 W/m², respectively, over the Indochina Peninsula. As discussed in Huang et al. (2023), aerosols derived from BB can ascend to altitudes of 2500–3000 m, which is close to the altitude of the Yunnan and Guizhou region in March. This leads to regional average

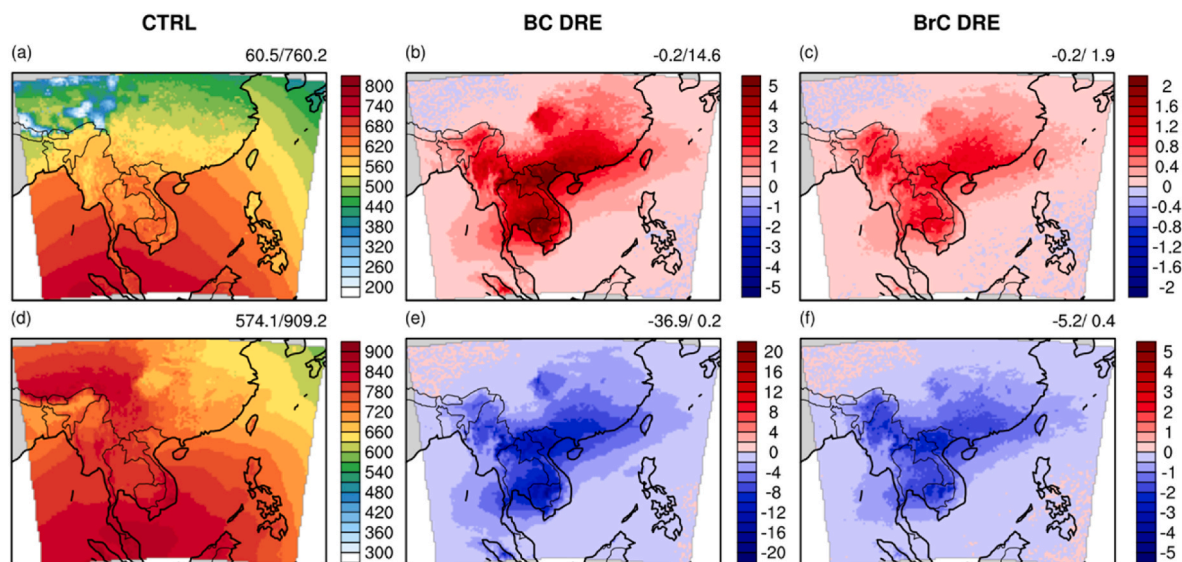


Fig. 4. (a–c) Monthly average clear sky net forcing at the top and (d–f) clear sky downward direct shortwave flux on the surface (unit: W/m^2) in March 2015. Values on the right upper corner of each subfigure indicates the minimum and maximum values, respectively.

changes caused by BC and BrC DRE of 1.9 and 0.6 W/m^2 , respectively. The southwesterlies dominate the free troposphere in this region, transporting BB pollutants northeastward to southern China. Additionally, the high altitude of the Yunnan and Tibetan Mountain ranges facilitates the transport of biomass pollutants to northern and eastern China under favorable wind conditions. This transportation belt can be well identified from the GD_GX region and HN island to TW island and even further regions (OTH). The regional average impact of BC and BrC DRE on GD_GX and HN regions are even higher than the Indo-CN region, with values of 3.7 and 0.9 W/m^2 , respectively. In the HN region, these impacts are 3.2 and 0.7 W/m^2 , respectively. Despite long-range transport, BC and BrC still have a considerable impact on TW, with regional average values of 2.0 and 0.5 W/m^2 , respectively. In the OTH region, the impact of BC and BrC can reach 12.7 and 1.8 W/m^2 , respectively, particularly in basin regions that tend to trap more air pollutants. However, the impacts on most OTH regions are generally smaller than those of other study regions, with average BC and BrC impacts of 0.7 and 0.2 W/m^2 , respectively. This is partly due to the OTH region being far from the BB source and not covered by the transport track of biomass pollutants. Additionally, BF emissions, which is allocated at the model's surface, have a shorter lifetime than BB emissions. As a result, the influence of BF emissions is generally less significant than that of BB emissions. Therefore, despite the considerable emissions from BF, the overall influence patterns are predominantly determined by the transport pathway of BB.

Focusing on the clear sky downward shortwave radiation at the surface, Fig. 4 (e, f) illustrate a similar but negative radiation change caused directly by the trapping of more shortwave radiation by lofted BC or BrC. The regional averages of shortwave flux reduction associated with BC DRE are -6.4 , -4.2 , -8.0 , -7.0 , -4.5 , and -1.7 W/m^2 , with regional maximum reaching as low as -36.9 , -12.3 , -10.2 , -8.4 , -6.3 , and -34.1 W/m^2 over Indo-CN, YN_GZ, GD_GX, HN, TW, and OTH regions, respectively. The regional average decreases in the shortwave flux owing to BrC DRE are -1.3 , -1.1 , -1.6 , -1.4 , -1.1 , and -0.4 W/m^2 , with regional maximum values of -5.2 , -2.2 , -2.2 , -1.7 , -1.6 , and -4.4 W/m^2 over Indo-CN, YN_GZ, GD_GX, HN, TW, and OTH, respectively.

3.1.2. Monthly variation

Fig. 5 and S3 show the monthly variations of clear sky net forcing at the top and downward direct shortwave flux on the surface caused by BC and BrC absorption DRE, along with their regional average percentage

contributions. The box and whisker plots represent the range of variation among grids in each study region. In order to present key information more effectively, data points above the 95th percentile and below the 5th percentile are excluded in Fig. 5 (a–f) and S3 (a–f). Thus, the bottom bar of the whisker represents the smallest 5% of the data, while the top bar represents the highest 5% of the data. The bottom and top bars of the box represent the 25th and 75th percentiles, respectively, and the middle bar of the box represents the average.

The concentrations of BC and OA can vary significantly on a daily basis (Fig. S2), leading to considerable variation in the impact of BC and BrC DRE, as illustrated in Fig. 5 (a–f) and S3 (a–f). Since the Indo-CN region is the source of BB emissions, the monthly span of the daily average net forcing at the top (represented by the middle bar of the box in the figures) is smaller in this region compared to others. During March 2015 (Fig. 5 (a)), the daily average net forcing at the top can range from 0.9 to 5.0 W/m^2 due to BC DRE and from 0.1 to 1.1 W/m^2 due to BrC DRE. When it comes to the daily average of the decrease in the shortwave flux, the value can range from -11.2 to -2.5 W/m^2 due to BC DRE and from -2.3 to -0.5 W/m^2 due to BrC DRE (Figure S3 (a)). The monthly spans of the average radiative impact are larger in the GD_GX, HN, and TW regions, reflecting the changing transport pathway of BB pollutants during March 2015. The impact of BC and BrC DRE is greater when the BB pollutants' transport pathway covers the study regions, while it is smaller when it does not. For instance, in the GD_GX region (Fig. 5 (c)), the daily average net forcing at the top due to BC DRE can be as low as 0.6 W/m^2 when not effected by BB pollutants, and the value can reach 10.4 W/m^2 when BB highly affects GD_GX region. Similarly, the daily average net forcing at the top can range from 0.1 to 2.4 W/m^2 due to BrC DRE. In addition, the daily average of the decrease in the shortwave flux can range from -21.1 to -1.1 W/m^2 due to BC DRE and from -4.3 to -0.3 W/m^2 due to BrC DRE (Figure S3 (c)). Similar large ranges can be observed in the HN (Figure S3 (d)) and TW (Figure S3 (e)) regions. Furthermore, the monthly variation in the YN_GZ region falls between that of the Indo-CN region and other study regions. Despite the monthly variations in the impact on radiation, the average percentage contributions of BC and BrC do not exhibit significant day-to-day variations in each study region (Fig. 5(g–l) and S3 (g–l)). Namely, the contribution ratio of BrC to BC remains relatively constant, generally ranging between 2:8 and 3:7.

During the pollution episode from March 18 to 22, 2015 (Fig. S3), higher BC and OC concentrations are observed over the main study regions. Correspondingly, larger BC and BrC DRE are also present during

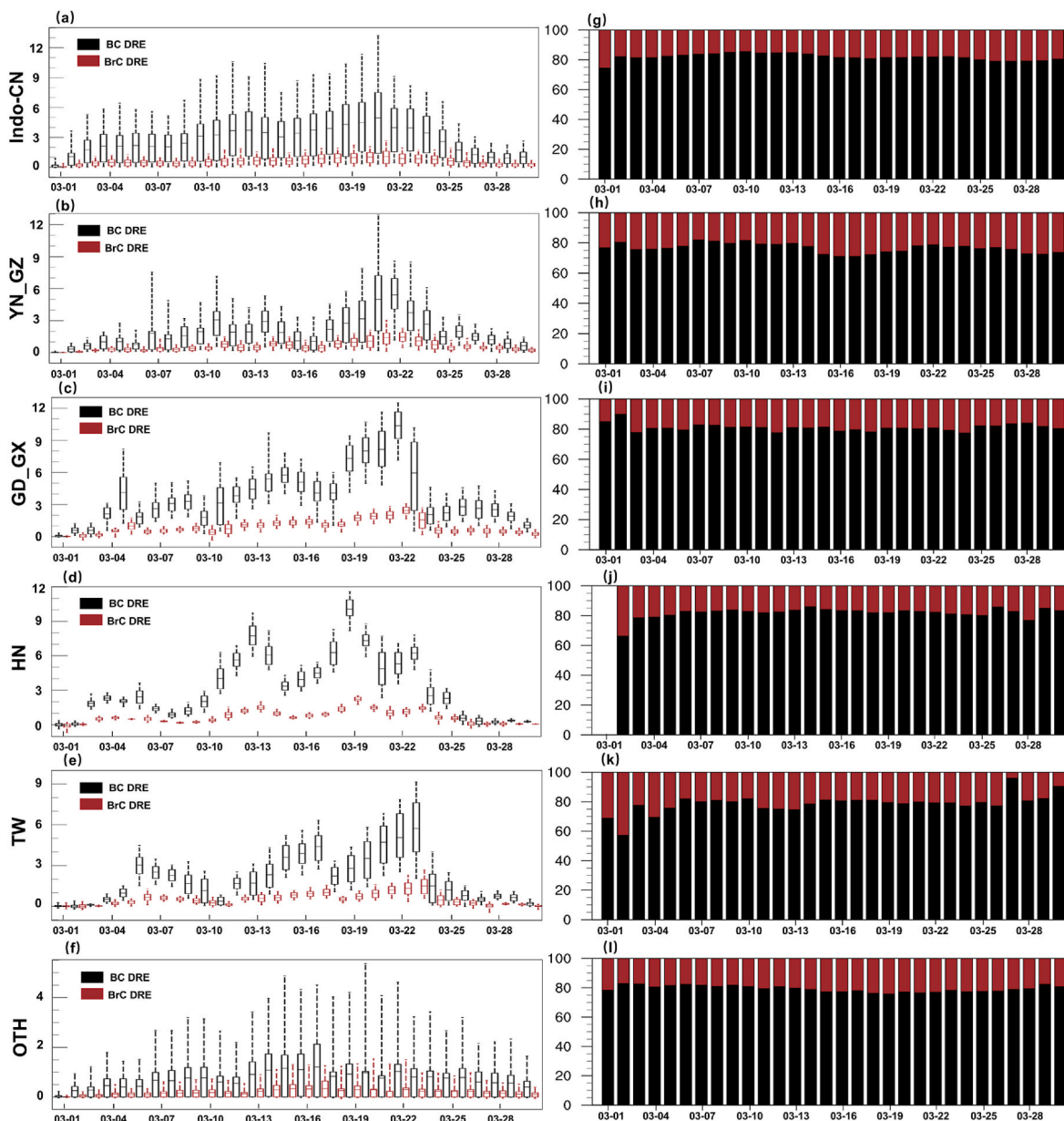


Fig. 5. (a–f) Daily variations of clear sky net forcing at the top caused by BC and BrC absorption directive radiative effect (unit: W/m^2) in six study regions and (g–l) their regional average percentage contributions.

this episode (Fig. 5 and S3). It is evident that a significant amount of BB pollutants originate from the Indo-CN region starting from March 17, and these pollutants are transported downstream to regions such as YN_GZ, HN island, and GD_GX, where BC and BrC concentrations start to rise on March 18 and peak on March 19. TW, being farther away from Indo-CN than other study regions, experienced the highest BC and BrC concentrations on March 20. Fig. S4 shows the average BC and BrC DRE during the pollution episode, demonstrating a substantial increase in the maximum clear sky net forcing at the top compared to the monthly average. The increase ranges from 14.6 to 23.9 W/m^2 caused due to BC absorption DRE and from 1.9 to 3.1 W/m^2 due to BrC absorption DRE. At the meanwhile, the maximum downward direct shortwave flux on the surface decreased from -36.9 to -68.2 W/m^2 due to BC absorption DRE and from -5.2 to -9.7 W/m^2 due to BrC absorption DRE, comparing the monthly average to pollution period average.

3.2. Impact on temperature

The warming and cooling effects are examined since the radiative forcing by the BC and BrC can directly warm up the atmosphere and cool the ground surface. This sector shows the influence of the BC and BrC DRE on daytime temperature in March 2015 (Fig. 6).

Fig. 6 (a) shows the 2-m temperature distribution over the simulated region, with tropical ocean surface temperature reaching around 25 °C, and most areas over Indo-CN having surface temperature above 30 °C. Fig. 6 (b, c) demonstrate a clear surface cooling effect over the Indo-CN to southern China region. The decrease in the shortwave flux results in a reduction in 2-m temperature over land areas. Less radiation is absorbed by the land, leading to less energy available to heat the near-surface air. Thus, the decrease in temperature patterns aligns with the reduction of shortwave flux. However, in terms of monthly means, the impact is relatively limited, with maximum reduction values reaching only -0.09 °C and -0.07 °C, respectively, due to BC and BrC DRE. More detailed information on maximum, minimum, and average values in the

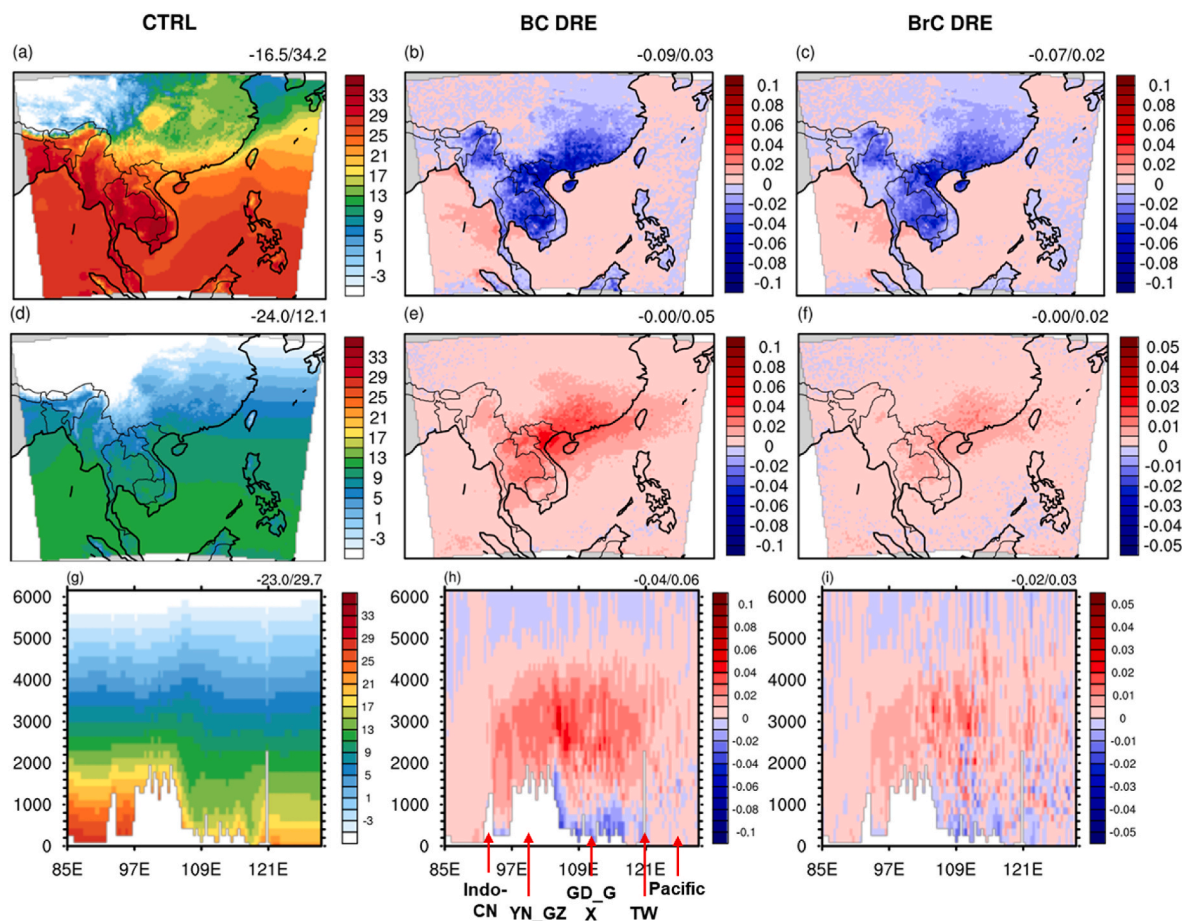


Fig. 6. BC and BrC direct radiative effect on monthly average daytime (a–c) surface temperature, (d–f) temperature in layer 23 (altitude of ~3,000 m), (g–i) temperature (unit: °C) in the west-east 24°N cross-section in March 2015. Values on the right upper corner of each subfigure indicate the minimum and maximum values, respectively.

six study regions can be found in Table S2. For example, the maximum regional temperature decreases due to BC DRE are -0.09 , -0.08 , -0.08 , -0.06 , -0.04 , and -0.06 °C over Indo-CN, YN_GZ, GD_GX, HN, TW, and OTH, respectively, while the maximum decreases owing to BrC DRE are -0.07 , -0.07 , -0.06 , -0.05 , -0.03 , and -0.04 °C, respectively, in March. In terms of regional averages, BC and BrC DRE have the largest impact in the GD_GX and HN regions, as these regions are mostly covered by the BB transport pathway, with GD_GX also experiencing considerable local BF emissions. Conversely, the surface temperature over the ocean increases due to the larger heat capacity ratio of the ocean, and the decrease in downward radiation has little effect on ocean temperature. Therefore, the heating effect caused by BC and BrC absorption is more efficient over the sea than over land.

Furthermore, BC and BrC absorb solar radiation, leading to heating of the atmosphere, particularly in model layer 23 (approximately 3000 m altitude above the surface; Fig. 6e and f). This layer represents the main height of the BB transport pathway, referring to Huang et al. (2023). Over the most significant region, BC heats the air by less than 0.05 °C, while the heating effect by BrC is much weaker, with a positive trend of no more than 0.02 °C.

To analyze the vertical profile of the BC and BrC heating effect, an air temperature cross-section plot along 24°N has been conducted. The cross-section figures (Fig. 6 (h and i)) reveal a significant aerosol cooling effect in the surface layer and a heating effect in the BB transport pathway. Fig. 6 (h) shows a warm core of 0.06 °C due to BC RDE extending from 105°E to 120°E, from 1000 m to 4500 m above the surface, covering large areas downstream of the mountainous region over the Indochina Peninsula. Similarly, a warming trend by BrC RDE is

vaguely discernible, indicating a positive but weak heating effect by BrC.

Figure S5 shows the influence of the BC and BrC DRE on daytime temperature during the pollution episode. Comparing Fig. 7 (e, f) and Figure S5 (e, f), a higher temperature increase during the pollution period indicates a stronger BC and BrC absorption effect due to higher concentrations of BC and BrC. The cooling effect at the surface due to BC DRE (Figure S5 (b)) also intensifies during the pollution period, while the cooling effect due to BrC DRE (Figure S5 (c)) weakens. In general, the impact of BC DRE on temperature can be significant during high-pollution periods, while the impact of BrC DRE remains limited.

3.3. Impact on ozone concentrations

The variations in the meteorological conditions are expected to influence the air quality (Fig. 7). Decreased solar radiation and temperature typically lead to decreased rates of photochemical reactions, while increased solar radiation and temperature accelerate these reactions. These phenomena partially explain the observed decrease in surface O₃ concentration. Fig. 7 (a) shows that the monthly mean daytime surface ozone concentration is high, ranging from 50 to 70 ppbv over the northern Indochina Peninsula to southwestern China, while it is around 40 ppbv over southern China. Fig. 7 (b) demonstrates that the BC DRE results in reduced shortwave radiation reaching the surface and lower surface temperatures, which in turn decreases ozone formation. The ozone concentration decreases by -0.8 ppbv over the Indo-CN (Table S2), where the impact of BC DRE is larger and the ozone concentration is higher. The largest BC DRE on ozone occurs in TW in March, with a maximum decrease of -1.0 ppbv. Although the BC DRE has a larger

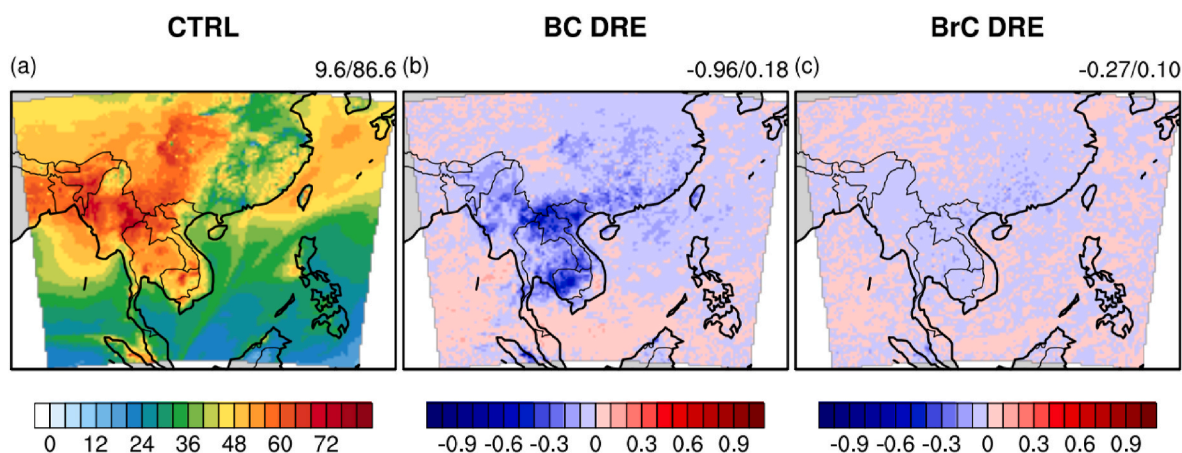


Fig. 7. BC and BrC direct radiative effect on average daytime surface O_3 concentration (unit: ppbv) in March 2015. Values on the right upper corner of each subfigure indicates the minimum and maximum values, respectively.

impact on the mean radiation in GD_GX and HN, its mean impact on ozone concentration is not significantly greater than in other regions due to the lower ozone concentration in these areas. Regarding the BrC effect on surface ozone (Fig. 7 (c)), the change is limited, with a maximum reduction of -0.3 ppb. However, the impact pattern of BrC DRE differs from that of BC DRE, showing a larger impact in GD_GX. This difference may be attributed to a higher BC to BrC ratio in the GD_GX region (Fig. S2), resulting in a larger BrC radiative impact. The impacts of BC and BrC DRE on surface ozone concentration are enhanced during the pollution period (Fig. S6) due to changes in radiation (Fig. S4). The negative impact of BC and BrC DRE on ozone can reach -1.8 and -0.8 ppbv, respectively.

4. Summary and discussion

The WRF-CMAQ two-way coupled modeling system embedded a parameterization scheme of the light absorption property of BrC was employed for the first time to investigate the BC and BrC absorption DRE over Southeast Asia in March 2015. Experiments with and without BC/BrC DRE were conducted, and the difference between control and sensitive experiments showed the impact of BC and BrC DRE.

Results show that the regional monthly mean impact on the clear sky net radiation at the top of the atmosphere can reach 14.6, 4.9, 5.1, 4.1, 2.9, and 12.7 W/m^2 due to BC DRE and 1.9, 1.1, 1.1, 0.9, 0.7, 1.8 W/m^2 due to BrC DRE over Indo-CN, YN_GZ, GD_GX, HN, TW, and OTH, respectively. These values are significantly larger than those reported in global studies over longer timescales, which indicated that the global annual average BC DRE impact ranged from $+0.2$ to $+0.9$ W/m^2 (Wang, 2004; Ramanathan and Carmichael, 2008; UNEP and WMO, 2011; Zhang et al., 2020), and the simulated BrC DRE ranged from $+0.03$ to $+0.6$ W/m^2 (Saleh et al., 2015; Brown et al., 2018; Wang et al., 2018; June et al., 2020; Drugé et al., 2022). For example, Wang et al. (2014) updated the BC and BrC with new but fixed absorption efficiencies, estimating global BC and BrC DRE values of 0.21 and 0.11 W/m^2 , respectively, using the global model GEOS-CHEM. To enhance model accuracy, they incorporated the BrC parameterization from Saleh et al. (2014) and reported updated global BC and BrC DRE values of 0.17 and 0.048 W/m^2 , respectively (Wang et al., 2018). Jo et al. (2016) assigned different modified combustion efficiencies (MCEs) to BrC for various BB source types based on McMeeking (2008) and found the global BrC DRE to be 0.11 W/m^2 . Zhang et al. (2020) estimated the global BrC DRE at 0.10 W/m^2 , exceeding 25% ($+0.39$ W/m^2) of BC, using the Community Atmosphere Model (CAM5) within the Community Earth System Model (CESM). It is worth noting that the impact of BC and BrC in the aforementioned studies exhibited significantly higher values over regions with extensive BB and BF activities, including Southeast Asia. Therefore,

in areas with high BB and BF emissions, especially during periods of strong BB activity such as wildfires, BrC DRF needs to be considered because it has a stronger contribution at this time. However, due to the lack of observational support and incomplete understanding of BrC, there are still variations in results among different studies caused by the various treatment methods applied to BrC emissions and optical properties.

On the other hand, BC and BrC DRE lead to a cooling effect at the Earth's surface, causing the regional maximum reduction on the clear sky downward shortwave radiation at surface reach -36.9 , -12.3 , -10.2 , -8.4 , -6.3 , and -34.1 W/m^2 due to BC DRE and -5.2 , -2.2 , -2.2 , -1.7 , -1.6 , and -4.4 W/m^2 due to BrC DRE over Indo-CN, YN_GZ, GD_GX, HN, TW, and OTH, respectively. This regional and synoptical scale cooling effect is significantly larger compared with long-term global effect shown in previous study (Feng et al., 2013), potentially playing a crucial role in surface temperatures and local climate, counterbalancing some of the warming effects associated with other greenhouse gases. From the monthly variation perspective, the BC and OA concentrations can exhibit significant day-to-day variations, which leads to considerable variation of impact from BC and BrC DRE. Meanwhile, the average percentage contributions of BC and BrC do not exhibit significant monthly variations, and the contribution ratio of BrC and BC generally range between 2:8 to 3:7.

The decrease in the shortwave flux decreased the 2-m temperature over the land. In contrast, the surface temperature over the ocean increased owing to the larger heat capacity ratio of the ocean. The impact on monthly 2-m temperature is relatively limited, and the maximum reduction values only reach -0.09 °C and -0.07 °C, respectively, due to BC and BrC DRE. Owing to the endothermic effect of BC and BrC DRE, the temperature at higher levels increased by up to 0.05 and 0.02 °C, respectively. Variations in the shortwave and temperature decreased the surface O_3 concentrations. The maximum reduction in O_3 concentration only reaches -1.0 ppbv by BC DRE, while the impact by BrC DRE is quite limited, with a maximum reduction of -0.3 ppb. During a pollution episode from March 18–22, higher concentrations of BC and OC are observed in the study regions, coinciding with larger BC and BrC DRE impacts. The impact of BC and BrC DRE during the pollution episode is nearly twice as significant as the monthly average. The impact on temperature and air quality should still be considered limited when conducting short-term and regional model studies.

The parameterization of BrC's absorption properties based on the BC/OA ratio represents a significant advancement over default coefficients. This approach aligns more closely with smog chamber experiments and enhances the accuracy of the model. In comparison to studies using the default coefficient, our research contributes to a more nuanced understanding of the interactions between BC, BrC, and

climate. For the WRF-CMAQ model which is widely used in local meteorological and air quality research, continuously improving the scientific validity and accuracy is beneficial for the related research and applications. This study provides new insights on the impacts of BrC DRE for WRF-CMAQ developers and users. Still, the parameterization of BrC's absorption properties based on the BC/OA ratio presents limitations: on the one hand, this approach relies on laboratory experiments, which may not fully capture the complex atmospheric conditions and variability in real-world scenarios; on the other hand, the lack of observational support and incomplete understanding of BrC for these parameters raises concerns about their applicability across different environments and burning conditions (Saleh, 2020; Li et al., 2023). At the same time, current research on BrC absorptivity is still developing, such as the daytime aging (photo-bleaching) and nighttime aging of BrC, where the former leads to a reduction in BrC absorptivity due to photobleaching and the latter enhances absorptivity through reaction with NO₃ (Lin et al., 2017; Wong et al., 2017; Hems and Abbatt, 2018; Li et al., 2019; Wong et al., 2019). Further atmospheric observations and laboratory experiments are essential to quantify or formulate the BrC scheme. Future studies should aim to incorporate field measurements and a broader range of parameterizations to enhance the robustness and applicability of BrC absorption modeling in diverse atmospheric contexts.

CRedit authorship contribution statement

Yeqi Huang: Writing – review & editing, Writing – original draft, Visualization, Validation, Software, Methodology, Investigation, Formal analysis, Data curation, Conceptualization. **Xingcheng Lu:** Writing – review & editing, Methodology, Investigation, Funding acquisition, Conceptualization. **Zhenning Li:** Writing – review & editing, Software. **Jimmy C.H. Fung:** Writing – review & editing, Supervision, Resources, Project administration, Funding acquisition. **Yuhang Wang:** Writing – review & editing. **Yiang Chen:** Writing – review & editing.

Declaration of competing interest

The authors declare that they have no known competing financial interests or personal relationships that could have appeared to influence the work reported in this paper.

Acknowledgments

This research was funded by the RGC Research Fund (Project No. 16302220), Guangdong-Hongkong-Macau Joint Laboratory of Collaborative Innovation for Environmental Quality (GDST2OIP05), MOST (Project No. 2023YFC3709200), United College Endowment Fund Research Grant, and Strategic Partnership Award for Research Collaboration from the Chinese University of Hong Kong.

Appendix A. Supplementary data

Supplementary data to this article can be found online at <https://doi.org/10.1016/j.envpol.2024.125425>.

Data availability

The authors do not have permission to share data.

References

Air Sciences, Inc., 2002. Fire Emission Inventory for the WRAP Region – Phase II, Prepared for the Western.
Andrae, M.O., Gelencsér, A., 2006. Black carbon or brown carbon? The nature of light-absorbing carbonaceous aerosols. *Atmos. Chem. Phys.* 6 (10), 3131–3148.

Bahadur, R., Praveen, P.S., Xu, Y., Ramanathan, V., 2012. Solar absorption by elemental and brown carbon determined from spectral observations. *Proc. Natl. Acad. Sci. USA* 109 (43), 17366–17371.
Bond, T.C., Bergstrom, R.W., 2006. Light absorption by carbonaceous particles: an investigative review. *Aerosol. Sci. Technol.* 40 (1), 27–67.
Bond, T.C., Doherty, S.J., Fahey, D.W., Forster, P.M., Bernsten, T., DeAngelo, B.J., Flanner, M.G., Ghan, S., Kärcher, B., Koch, D., Kinne, S., 2013. Bounding the role of black carbon in the climate system: a scientific assessment. *J. Geophys. Res. Atmos.* 118 (11), 5380–5552.
Bond, T.C., Zarzycki, C., Flanner, M.G., Koch, D.M., 2011. Quantifying immediate radiative forcing by black carbon and organic matter with the Specific Forcing Pulse. *Atmos. Chem. Phys.* 11 (4), 1505–1525.
Brown, H., Liu, X., Feng, Y., Jiang, Y., Wu, M., Lu, Z., Wu, C., Murphy, S., Pokhrel, R., 2018. Radiative effect and climate impacts of brown carbon with the Community Atmosphere Model (CAM5). *Atmos. Chem. Phys.* 18 (24), 17745–17768.
Charlson, R.J., Schwartz, S.E., Hales, J.M., Cess, R.D., Coakley Jr, J.A., Hansen, J.E., Hofmann, D.J., 1992. Climate forcing by anthropogenic aerosols. *Science* 255 (5043), 423–430.
Chen, J., Li, C., Ristovski, Z., Milic, A., Gu, Y., Islam, M.S., Wang, S., Hao, J., Zhang, H., He, C., Guo, H., 2017. A review of biomass burning: emissions and impacts on air quality, health and climate in China. *Sci. Total Environ.* 579, 1000–1034.
Cheng, Z., Wang, S., Fu, X., Watson, J.G., Jiang, J., Fu, Q., Chen, C., Xu, B., Yu, J., Chow, J.C., Hao, J., 2014. Impact of biomass burning on haze pollution in the Yangtze River delta, China: a case study in summer 2011. *Atmos. Chem. Phys.* 14 (9), 4573–4585.
Chung, C.E., Kim, S.W., Lee, M., Yoon, S.C., Lee, S., 2012. Carbonaceous aerosol AAE inferred from in-situ aerosol measurements at the Gosan ABC super site, and the implications for brown carbon aerosol. *Atmos. Chem. Phys.* 12 (14), 6173–6184.
Crippa, Monica, Guizzardi, Diego, Muntean, Marilena, Schaaf, Edwin, Oreggioni, Gabriel, 2019. EDGAR v5.0 global air pollutant emissions. In: European Commission. Joint Research Centre (JRC) PID. <http://data.europa.eu/89h/377801a-f-b094-4943-8fde-f79a7c0c2d19>.
Crippa, M., Solazzo, E., Huang, G., Guizzardi, D., Koffi, E., Muntean, M., Schieberle, C., Friedrich, R., Janssens-Maenhout, G., 2020. High resolution temporal profiles in the emissions database for global atmospheric research. *Sci. Data* 7 (1), 1–17.
Cui, J., Tian, H., Qi, Y., Hu, X., Li, S., Zhang, W., Wei, Z., Zhang, M., Liu, Z., Abolfathi, S., 2024. Impact of microplastic residues from polyurethane films on crop growth: unraveling insights through transcriptomics and metabolomics analysis. *Ecotoxicol. Environ. Saf.* 283, 116826.
Dong, X., Fu, J.S., 2015. Understanding interannual variations of biomass burning from Peninsular Southeast Asia, part II: variability and different influences in lower and higher atmosphere levels. *Atmos. Environ.* 115, 9–18.
Drüge, T., Nabat, P., Mallet, M., Michou, M., Rémy, S., Dubovik, O., 2022. Modeling radiative and climatic effects of brown carbon aerosols with the ARPEGE-Climate global climate model. *Atmos. Chem. Phys.* 22 (18), 12167–12205.
Feng, Y., Ramanathan, V., Kotamarthi, V.R., 2013. Brown carbon: a significant atmospheric absorber of solar radiation? *Atmos. Chem. Phys.* 13 (17), 8607–8621.
Guenther, A., Jiang, X., Shah, T., Huang, L., Kemball-Cook, S., Yarwood, G., 2020. Model of emissions of gases and aerosol from nature version 3 (MEGAN3) for estimating biogenic emissions. In: *Air Pollution Modeling and its Application XXVI 36*. Springer International Publishing, pp. 187–192.
Guyon, P., Frank, G.P., Welling, M., Chand, D., Artaxo, P., Rizzo, L., Nishioka, G., Kolle, O., Fritsch, H., Silva Dias, M.F., Gatti, L.V., 2005. Airborne measurements of trace gas and aerosol particle emissions from biomass burning in Amazonia. *Atmos. Chem. Phys.* 5 (11), 2989–3002.
Hansen, J., Sato, M.K.I., Ruedy, R., Nazarenko, L., Lacis, A., Schmidt, G.A., Russell, G., Aleinov, I., Bauer, M., Bauer, S., Bell, N., 2005. Efficacy of climate forcings. *J. Geophys. Res. Atmos.* 110 (D18).
Hecobian, A., Zhang, X., Zheng, M., Frank, N., Edgerton, E.S., Weber, R.J., 2010. Water-Soluble Organic Aerosol material and the light-absorption characteristics of aqueous extracts measured over the Southeastern United States. *Atmos. Chem. Phys.* 10 (13), 5965–5977.
Hems, R.F., Abbatt, J.P., 2018. Aqueous phase photo-oxidation of brown carbon nitrophenols: reaction kinetics, mechanism, and evolution of light absorption. *ACS Earth Space Chem.* 2 (3), 225–234.
Hess, M., Koepke, P., Schult, I., 1998. Optical properties of aerosols and clouds: the software package OPAC. *Bull. Am. Meteorol. Soc.* 79 (5), 831–844.
Huang, Y., Deng, T., Li, Z., Wang, N., Yin, C., Wang, S., Fan, S., 2018. Numerical simulations for the sources apportionment and control strategies of PM_{2.5} over Pearl River Delta, China, part I: inventory and PM_{2.5} sources apportionment. *Sci. Total Environ.* 634, 1631–1644.
Huang, Y., Lu, X., Fung, J.C., Sarwar, G., Li, Z., Li, Q., Saiz-Lopez, A., Lau, A.K., 2021. Effect of bromine and iodine chemistry on tropospheric ozone over Asia-Pacific using the CMAQ model. *Chemosphere* 262, 127595.
Huang, Y., Lu, X., Fung, J.C., Wong, D.C., Li, Z., Chen, Y., Chen, W., 2023. Investigating Southeast Asian biomass burning by the WRF-CMAQ two-way coupled model: emission and direct aerosol radiative effects. *Atmos. Environ.* 294, 119521.
Jo, D.S., Park, R.J., Lee, S., Kim, S.W., Zhang, X., 2016. A global simulation of brown carbon: implications for photochemistry and direct radiative effect. *Atmos. Chem. Phys.* 16 (5), 3413–3432.
Johnston, F.H., Henderson, S.B., Chen, Y., Randerson, J.T., Marlier, M., DeFries, R.S., Kinney, P., Bowman, D.M., Brauer, M., 2012. Estimated global mortality attributable to smoke from landscape fires. *Environ. Health Perspect.* 120 (5), 695–701.
June, N.A., Wang, X., Chen, L.W.A., Chow, J.C., Watson, J.G., Wang, X., Henderson, B.H., Zheng, Y., Mao, J., 2020. Spatial and temporal variability of brown carbon in the

- United States: implications for direct radiative effects. *Geophys. Res. Lett.* 47 (23), e2020GL090332.
- Kirchstetter, T.W., Thatcher, T.L., 2012. Contribution of organic carbon to wood smoke particulate matter absorption of solar radiation. *Atmos. Chem. Phys.* 12 (14), 6067–6072.
- Kurokawa, J., Ohara, T., 2020. Long-term historical trends in air pollutant emissions in Asia: regional Emission inventory in ASIA (REAS) version 3. *Atmos. Chem. Phys.* 20 (21), 12761–12793.
- Li, C., He, Q., Hettiyadura, A.P.S., Kafer, U., Shmul, G., Meidan, D., Zimmermann, R., Brown, S.S., George, C., Laskin, A., Rudich, Y., 2019. Formation of secondary brown carbon in biomass burning aerosol proxies through NO₃ radical reactions. *Environ. Sci. Technol.* 54 (3), 1395–1405.
- Li, J., Han, Z., Surapipith, V., Fan, W., Thongboonchoo, N., Wu, J., Li, J., Tao, J., Wu, Y., Macatangay, R., Bran, S.H., 2022. Direct and indirect effects and feedbacks of biomass burning aerosols over Mainland Southeast Asia and South China in springtime. *Sci. Total Environ.* 842, 156949.
- Li, M., Wang, T., Xie, M., Li, S., Zhuang, B., Chen, P., Huang, X., Han, Y., 2018. Agricultural fire impacts on ozone photochemistry over the Yangtze River Delta region, East China. *J. Geophys. Res. Atmos.* 123 (12), 6605–6623.
- Li, S., Zhang, H., Wang, Z., Chen, Y., 2023. Advances in the research on brown carbon aerosols: its concentrations, radiative forcing, and effects on climate. *Aerosol Air Qual. Res.* 23 (8), 220336.
- Lin, C.Y., Zhao, C., Liu, X., Lin, N.H., Chen, W.N., 2014. Modelling of long-range transport of Southeast Asia biomass-burning aerosols to Taiwan and their radiative forcings over East Asia. *Tellus B* 66 (1), 23733.
- Lin, P., Bluvshstein, N., Rudich, Y., Nizkorodov, S.A., Laskin, J., Laskin, A., 2017. Molecular chemistry of atmospheric brown carbon inferred from a nationwide biomass burning event. *Environ. Sci. Technol.* 51 (20), 11561–11570.
- Moosmüller, H., Chakrabarty, R.K., Arnott, W.P., 2009. Aerosol light absorption and its measurement: a review. *J. Quant. Spectrosc. Radiat. Transf.* 110 (11), 844–878.
- Mukai, H., Ambe, Y., 1986. Characterization of a humic acid-like brown substance in airborne particulate matter and tentative identification of its origin. *Atmos. Environ.* 20 (5), 813–819, 1967.
- Park, R.J., Kim, M.J., Jeong, J.I., Youn, D., Kim, S., 2010. A contribution of brown carbon aerosol to the aerosol light absorption and its radiative forcing in East Asia. *Atmos. Environ.* 44 (11), 1414–1421.
- Pöschl, U., 2005. Atmospheric aerosols: composition, transformation, climate and health effects. *Angew. Chem. Int. Ed.* 44 (46), 7520–7540.
- Qin, Y.M., Tan, H.B., Li, Y.J., Li, Z.J., Schurman, M.I., Liu, L., Wu, C., Chan, C.K., 2018. Chemical characteristics of brown carbon in atmospheric particles at a suburban site near Guangzhou, China. *Atmos. Chem. Phys.* 18 (22), 16409–16418.
- Ramanathan, V., Carmichael, G., 2008. Global and regional climate changes due to black carbon. *Nat. Geosci.* 1 (4), 221–227.
- Randerson, J.T., van der Werf, G.R., Giglio, L., Collatz, G.J., Kasibhatla, P.S., 2017. **Global Fire Emissions Database, Version 4.1 (GFEDv4)**. ORNL DAAC, Oak Ridge, Tennessee, USA. <https://doi.org/10.3334/ORNLDAAC/1293>.
- Reddington, C.L., Conibear, L., Robinson, S., Knote, C., Arnold, S.R., Spracklen, D.V., 2021. Air pollution from forest and vegetation fires in Southeast Asia disproportionately impacts the poor. *GeoHealth* 5 (9), e2021GH000418.
- Saleh, R., 2020. From measurements to models: toward accurate representation of brown carbon in climate calculations. *Curr. Pollut. Rep.* 6, 90–104.
- Saleh, R., Cheng, Z., Atwi, K., 2018. The brown–black continuum of light-absorbing combustion aerosols. *Environ. Sci. Technol. Lett.* 5 (8), 508–513.
- Saleh, R., Marks, M., Heo, J., Adams, P.J., Donahue, N.M., Robinson, A.L., 2015. Contribution of brown carbon and lensing to the direct radiative effect of carbonaceous aerosols from biomass and biofuel burning emissions. *J. Geophys. Res. Atmos.* 120 (19), 10–285.
- Saleh, R., Robinson, E.S., Tkacik, D.S., Ahern, A.T., Liu, S., Aiken, A.C., Sullivan, R.C., Presto, A.A., Dubey, M.K., Yokelson, R.J., Donahue, N.M., Robinson, A.L., 2014. Brownness of organics in aerosols from biomass burning linked to their black carbon content. *Nat. Geosci.* 7 (9), 647–650.
- Saleh, R.C.J.H., Hennigan, C.J., McMeeking, G.R., Chuang, W.K., Robinson, E.S., Coe, H., Donahue, N.M., Robinson, A.L., 2013. Absorptivity of brown carbon in fresh and photo-chemically aged biomass-burning emissions. *Atmos. Chem. Phys.* 13 (15), 7683–7693.
- Takami, K., Shimadaira, H., Uranishi, K., Kondo, A., 2020. Impacts of biomass burning emission inventories and atmospheric reanalyses on simulated PM₁₀ over Indochina. *Atmosphere* 11 (2), 160.
- Tian, H., Du, Y., Luo, X., Dong, J., Chen, S., Hu, X., Zhang, M., Liu, Z., Abolfathi, S., 2024a. Understanding visible light and microbe-driven degradation mechanisms of polyurethane plastics: pathways, property changes, and product analysis. *Water Res.*, 121856.
- Tian, H., Wang, L., Zhu, X., Zhang, M., Li, L., Liu, Z., Abolfathi, S., 2024b. Biodegradation of microplastics derived from controlled release fertilizer coating: selective microbial colonization and metabolism in plastisphere. *Sci. Total Environ.* 920, 170978.
- UNEP and WMO, 2011. **Integrated assessment of black carbon and tropospheric ozone. By the United Nations Environment Programme and World Meteorological Organization**. Available at: <https://www.ccaoalition.org/resources/integrated-assessment-black-carbon-and-tropospheric-ozone#:~:text=Integrated%20Assessment%20of%20Black%20Carbon%20and%20Tropospheric%20Ozone,-Publi shed&text=Scientific%20evidence%20and%20new%20analyses,benefits%20for%20human%20well%2Db eing.>
- US Environmental Protection Agency (US EPA), 2012. Report to Congress on Black Carbon. Office of Air Quality Planning and Standards, Office of Atmospheric Programs, Office of Radiation and Indoor Air, Office of Research and Development, Office of Transportation and Air Quality, Washington, DC. EPA-450/R-12-001.
- van Marle, M.J., Kloster, S., Magi, B.I., Marlon, J.R., Daniiau, A.L., Field, R.D., Arneth, A., Forrest, M., Hantson, S., Kehrwald, N.M., Knorr, W., 2017. Historic global biomass burning emissions for CMIP6 (BB4CMIP) based on merging satellite observations with proxies and fire models (1750–2015). *Geosci. Model Dev. (GMD)* 10 (9), 3329–3357.
- Wang, C., 2004. A modeling study on the climate impacts of black carbon aerosols. *J. Geophys. Res. Atmos.* 109 (D3).
- Wang, X., Heald, C.L., Liu, J., Weber, R.J., Campuzano-Jost, P., Jimenez, J.L., Schwarz, J.P., Perring, A.E., 2018. Exploring the observational constraints on the simulation of brown carbon. *Atmos. Chem. Phys.* 18 (2), 635–653.
- Wang, X., Heald, C.L., Ridley, D.A., Schwarz, J.P., Spackman, J.R., Perring, A.E., Coe, H., Liu, D., Clarke, A.D., 2014. Exploiting simultaneous observational constraints on mass and absorption to estimate the global direct radiative forcing of black carbon and brown carbon. *Atmos. Chem. Phys.* 14 (20), 10989–11010.
- Wang, X., Heald, C.L., Sedlacek, A.J., de Sá, S.S., Martin, S.T., Alexander, M.L., Watson, T.B., Aiken, A.C., Springston, S.R., Artaxo, P., 2016. Deriving brown carbon from multiwavelength absorption measurements: method and application to AERONET and Aethalometer observations. *Atmos. Chem. Phys.* 16 (19), 12733–12752.
- Wong, D.C., Pleim, J., Mathur, R., Binkowski, F., Otte, T., Gilliam, R., Pouliot, G., Xiu, A., Young, J.O., Kang, D., 2012. WRF-CMAQ two-way coupled system with aerosol feedback: software development and preliminary results. *Geosci. Model Dev. (GMD)* 5 (2), 299–312.
- Wong, J.P., Nenes, A., Weber, R.J., 2017. Changes in light absorptivity of molecular weight separated brown carbon due to photolytic aging. *Environ. Sci. Technol.* 51 (15), 8414–8421.
- Wong, J.P., Tsagkaraki, M., Tsiodra, I., Mihalopoulos, N., Violaki, K., Kanakidou, M., Sciare, J., Nenes, A., Weber, R.J., 2019. Atmospheric evolution of molecular-weight separated brown carbon from biomass burning. *Atmos. Chem. Phys.* 19 (11), 7319–7334.
- Wu, G.M., Cong, Z.Y., Kang, S.C., Kawamura, K., Fu, P.Q., Zhang, Y.L., et al., 2016. Brown carbon in the cryosphere: current knowledge and perspective. *Adv. Clim. Change Res.* 7 (1), 82–89.
- Wu, J., Fu, C., Xu, Y., Tang, J.P., Wang, W., Wang, Z., 2008. Simulation of direct effects of black carbon aerosol on temperature and hydrological cycle in Asia by a Regional Climate Model. *Meteorol. Atmos. Phys.* 100, 179–193.
- Xie, M., Shen, G., Holder, A.L., Hays, M.D., Jetter, J.J., 2018. Light absorption of organic carbon emitted from burning wood, charcoal, and kerosene in household cookstoves. *Environ. Pollut.* 240, 60–67.
- Yan, J., Wang, X., Gong, P., Wang, C., Cong, Z., 2018. Review of brown carbon aerosols: recent progress and perspectives. *Sci. Total Environ.* 634, 1475–1485.
- Zhang, A., Wang, Y., Zhang, Y., Weber, R.J., Song, Y., Ke, Z., Zou, Y., 2020. Modeling the global radiative effect of brown carbon: a potentially larger heating source in the tropical free troposphere than black carbon. *Atmos. Chem. Phys.* 20 (4), 1901–1920.
- Zhang, H., Wang, Z., Guo, P., Wang, Z., 2009. A modeling study of the effects of direct radiative forcing due to carbonaceous aerosol on the climate in East Asia. *Adv. Atmos. Sci.* 26, 57–66.
- Zhang, Y., Forrister, H., Liu, J., Dibb, J., Anderson, B., Schwarz, J.P., Perring, A.E., Jimenez, J.L., Campuzano-Jost, P., Wang, Y., Nenes, A., 2017. Top-of-atmosphere radiative forcing affected by brown carbon in the upper troposphere. *Nat. Geosci.* 10 (7), 486–489.